Politecnico di Milano

Smart Structures and Devices

REPORT

Option I: Hybrid Metastructure

Students:

Rui Sobreira Amorim de Sousa - 10756181

Kavinda Pradeep Herath Herath Mudiyanselage - 10730809

A.Y. 2020/2021

Content

1. Objective

The objective of this project is to study bandgap formation due to mechanical and electromechanical resonators on metastructure. In order to achieve the above target, we derived general analytical solution for the hybrid system with and without damping and observed the bandgap formation through numerical procedure. The hybrid metastructure is excited by the base vibration and linear bending force. To derive analytical solution, we use the modal shapes of the structure without the resonators and calculate a modifying function to account the resonators. At last, the potential to harvest energy through electromechanical resonators was explored and its effect on the bandgap formation analysed. Reference of the original literature [1].

2. Terminology

Terms	Meanings
ω	Relative transverse displacement
k_j	Stiffness of the attached mass
m_j	Mass attached
u_j	Relative displacement of the beam
$\delta(x - x_j)$	Dirac function
v_j	Voltage across the circuit of jth electrode
$H(x)$	Heaviside function
$f(x,t)$	Linear bending force
ω_b	Transverse displacement of the base
y_j	linear integro-differential operator corresponding to the admittance of the jth electrodes
b	Width of the beam and the electrode
c_S	Elastic modules of the substrate
H_S	Thickness of the substrate
$\bar{c}_{11}^E$	Inverse of the electric compliance at constant electric field
h_p	Thickness of the piezoelectric material
ρ_S	Density of the substrate
ρ_p	Density of the piezoelectric material
$\bar{e}_{31}$	Ratio between the piezoelectric strain constant and electric compliance
$\bar{\varepsilon}_{33}^S$	Difference of permittivity constant and ratio between the piezoelectric strain constant and electric compliance
Δx_j	Length of the electrode
μ	Ratio of total mass added to the mass of the bimorph beam
N	Number of modes
$\phi(x)$	Mass normalised modal shape of the plain structure
$\eta(t)$	Modal weighting
H(s)	$\eta(t)$ in the Laplace domain
$U_j(s)$	$u_j(t)$ in the Laplace domain

$V_j(s)$	$v_j(t)$ in the Laplace domain
$W_b(s)$	$\omega_b(t)$ in the Laplace domain
ω_t	Control frequency from mechanical resonator
ω_t	Control frequency from electromechanical resonator
α	Electromechanical coupling
L	Length of the beam
h_s	Thickness of the substrate material
λ_r	rth solution of the characteristic equation
r	rth mode
ζ	Damping ratio of mechanical resonator

3. General theory of the band formation of hybrid metastructure

In this project, the structure we considered was a bimorph beam. The beam is clamped on one side and free on the other end. The mechanical resonators are placed at equal distance, and they are consistent of the same mass and the stiffness. For the simplicity at the beginning damping is neglected and damping is introduced later, and a comparison is made. The beam is fully covered both top and bottom with the piezoelectric material as shown by the dark grey area in figure 1. The electrodes are placed on the top and bottom of the beam with an infinitesimal spacing. The electrodes are connected to the inductor through serial connection. The piezoelectric material was assumed place on the beam considering polling direction to facilitate the above configuration. A segment of the electromechanical and mechanical resonator configuration is shown in figure 1.
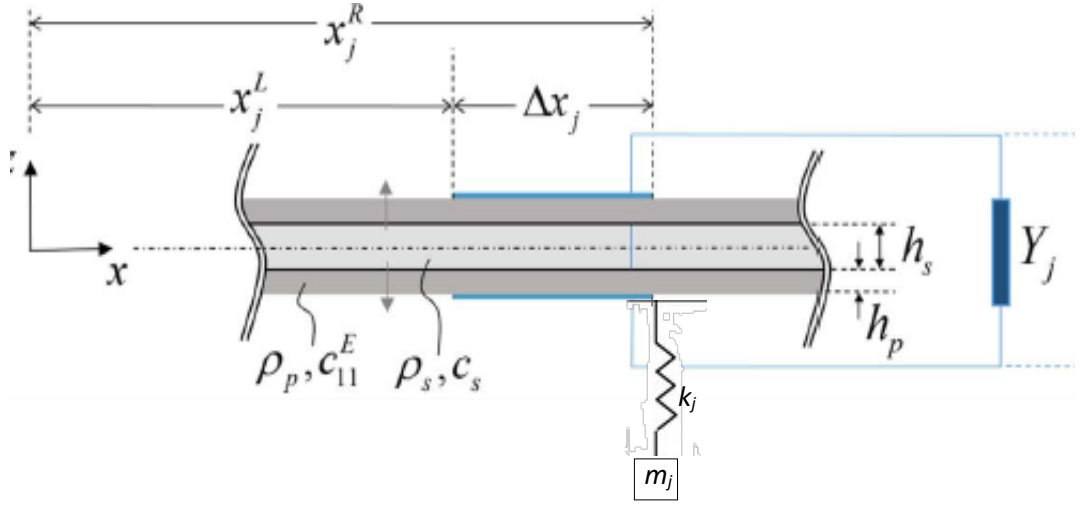

Figure 1 electromechanical and mechanical resonator schematic [1]

We can write the electromechanical equation for the beam, equation of motion for the mechanical resonator and equation of current balance for the circuit. These equations are given by the equations 1, 2, and 3 respectively.

$$EI\frac{\partial^4 \omega}{\partial x^4} + m\frac{\partial^2 \omega}{\partial t^2} - \sum_{j=1}^{S}(k_j u_j)\delta(x - x_j^R) - \theta\sum_{j=1}^{S} v_j(t)\frac{\partial^2}{\partial x^2}\left[H(x - x_j^L) - H(x - x_j^R)\right]$$
$$= f(x,t) - m\ddot{\omega}_b \tag{1}$$

$$m_j\ddot{u}_j + k_j u_j(t) + m_j\ddot{\omega}(x_j^R, t) = -m_j\ddot{\omega}_b \tag{2}$$

$$C_{p,j}\,\dot{v}_j(t) + y_j\big[v_j(t)\big] + \theta \int_{x_j^L}^{x_j^R} \frac{\partial^3 \omega}{\partial x^2\,\partial t}\,dx = 0 \tag{3}$$

In above equations the terms EI, m, θ and $C_{p,j}$ are given by the equations 4, 5, 6 and 7. The subscript j is used to denote the generic mechanical and electromechanical resonator.

$$EI = \frac{2b}{3}\left(c_S \frac{h_S^3}{8} + \bar{c}_{11}^E\left[\left(h_p + \frac{h_S}{2}\right)^3 - \frac{h_S^3}{8}\right]\right) \tag{4}$$

$$m = b(\rho_S h_S + 2\rho_p h_p) \tag{5}$$

$$\theta = \frac{\bar{e}_{31} b}{2h_p}\left[\left(h_p + \frac{h_S}{2}\right)^2 - \frac{h_S^2}{4}\right] \tag{6}$$

$$C_{p,j} = \frac{\bar{\varepsilon}_{33}^S b \Delta x_j}{2h_p} \tag{7}$$

In deriving analytical solution several assumptions are drawn. We assumed that width of the electrode and bimorph beam is equal, given as b. We assume that structure contains S number of hybrid resonators. The length of the electrode is given by $\frac{L}{S}$, which is Δx_j. The mass of mechanical resonator is m_j which is equal to $\mu \frac{mL}{S}$. μ is the ratio between the total mass added vs the mass of the plain structure.

By using an assumed mode expansion with N modes as shown in the equation 8, we can obtain the equation 9, 10 and 11. Equations 9, 10 and 11 can be obtain simply substituting equation 8 in equations 1, 2 and 3. Here $\phi(x)$ is a mass normalized modal shape of the structure without the resonator (plain structure). Here $\phi(x)$ is acting as the basis function. More about this function is discussed in section 8.a. And $\eta(t)$ is the modal coordinates that need to determine. The subscript r corresponds to the rth mode.

$$\omega(x,t) = \sum_{r=1}^{N} \phi_r(x)\,\eta_r(t) \tag{8}$$

6

$$EI \sum_{r=1}^{N} \phi_r''''(x)\eta_r(t) + m \sum_{r=1}^{N} \phi_r \, \ddot{\eta}_r$$
$$- \sum_{j=1}^{S} (k_j u_j)\delta(x - x_j^R) - \theta \sum_{j=1}^{S} v_j(t) \frac{\partial^2}{\partial x} [H(x - x_j^L) - H(x - x_j^R)]$$
$$= f(x,t) - m\ddot{w}_b \tag{9}$$

$$m_j \ddot{u}_j + k_j u_j(t) + m_j \sum_{k=1}^{N} \phi_k(x_j^R)\ddot{\eta}_k = -m_j \ddot{w}_b \tag{10}$$

$$C_{p,j} \, \dot{v}_j(t) + y_j[v_j(t)] + \theta \sum_{k=1}^{N} \int_{x_j^L}^{x_j^R} \phi_k''(x)\dot{\eta}_k dx = 0 \tag{11}$$

In equations 10 and 11 instead of r term k is used since it is useful to distinct the terms under summation in further steps. We exploit orthogonality property on equation 9 by multiply the left-hand side and the right-hand side by $\phi_s(x)$ and integrating from 0 to L, obtaining the equation 14. The orthogonal properties are given by the equations 12 and 13. ω_r is the natural frequency of the rth mode of the plain structure. δ_{rk} is the Kronecker delta which is equal to one when $r = s$.

$$\int_0^L m\phi_r(x)\phi_s(x)dx = \delta_{rs} \tag{12}$$

$$\int_0^L EI\phi_s(x)\frac{d^4\phi_r(x)}{dx^4}dx = \omega_r^2\delta_{rs} \tag{13}$$

$$\ddot{\eta}_r + \omega_r\eta_r(t) + \sum_{j=1}^{S} k_j u_j \phi_s(x_j^R) - \theta \sum_{j=1}^{S} u_j(t)\left[\frac{d\phi_r}{dx}\right]_{x_j^L}^{x_j^R} = \int_0^L (f(x,t) - m\ddot{w}_b)\phi(x)dx \tag{14}$$

We can bring the equation 14, 10 and 11 into the Laplace domain and they are given by the equations 15, 16 and 17. $H(s)$ is the $\eta(t)$ in the Laplace domain, $U_j(s)$ is the $u_j(t)$ in the Laplace domain, $V_j(s)$ is the $v_j(t)$ in the Laplace domain, $W_b(s)$ is the $w_b(t)$ in Laplace domain, Y_j is the y_j in the Laplace domain and $F(x,s)$ is the $f(x,t)$ in the Laplace domain .

$$H_r(s)[s^2 + \omega_r^2] + \sum_{j=1}^{S} k_j\, \phi_s(x_j)U_j(s) - \theta \sum_{j=1}^{S} V_j(s)\left[\frac{d\phi_s}{dx}\right]_{x_j^L}^{x_j^R} = F(x,s) - ms^2 W_b(s)dx \tag{15}$$

$$\left(m_j s^2 + k_j\right)U_j(s) + m_j \sum_{k=1}^{N} \phi_k(x_j^R)s^2\, H_k(s) = -m_j s^2 W_b(s) \tag{16}$$

$$[c_{p,j}\, s + Y_j]V_j(s) + \theta \sum_{k=1}^{N}\left[\frac{d\phi_k}{dx}\right]_{x_j^L}^{x_j^R} sH_k(s) = 0 \tag{17}$$

We can substitute the equations 16 and 17 into equation 15 and obtain the equation 18 and we can substitute k_j with $\omega_{tj}^2 m_j$, where m_j, k_j and ω_{tj} are mass, stiffness and the natural frequency of a jth mechanical resonator respectively.

$$H_r(s)[s^2 + \omega_r^2] + \sum_{j=1}^{S}\sum_{k=1}^{N} \frac{\omega_{tj}^2 m_j \phi_k(x_j^R)\phi_s(x_j^R)s^2}{s^2 + \omega_{tj}^2} H_k(s)$$

$$+ \theta \sum_{j=1}^{S}\sum_{k=1}^{N} \frac{s}{c_{p,j}\, s + Y_j(s)}\left[\frac{d\phi_k}{dx}\right]_{x_j^L}^{x_j^R}\left[\frac{d\phi_s}{dx}\right]_{x_j^L}^{x_j^R} H_k(s)$$

$$= \int_0^L F(x,s)\phi(x)dx - \left(\int_0^L ms^2\phi(x)dx + \sum_{j=1}^{S} \frac{\phi_s(x_j^R)\omega_{tj}^2 m_j s^2}{s^2 + \omega_{tj}^2}\right)W_b(s) \tag{18}$$

Having same mass and stiffness at every resonator, we can say that natural frequencies of all the resonator are equal and we can move the natural frequency out of the summation and it can be named as ω_t. This frequency is affecting the frequency at which bandgap is formed and it can be adjusted by changing the added stiffness and resonator mass according to the equation $\sqrt{\frac{k_j}{m_j}}$. Here we fixed resonator mass hence ω_t is only adjusted by changing the stiffness. Similarly having an equal length of the electrodes, same piezoelectric material throughout the beam and same inductor used, we can move the capacitance and the term due to admittance of the jth electrode couple out of the summation. we will be calling these terms c_p and $Y(s)$ respectively. This new equation is given by equation number 19.

$$H_r(s)[s^2 + \omega_r^2] + \frac{\omega_t^2 s^2}{s^2 + \omega_t^2} \sum_{k=1}^{N} \sum_{j=1}^{S} m_j \, \phi_s(x_j)\phi_k(x_j)H_k(s)$$

$$+ \frac{\theta s}{c_p s + Y(s)} \sum_{k=1}^{N} \sum_{j=1}^{S} \left[\frac{d\phi_k}{dx}\right]_{x_j^L}^{x_j^R} \left[\frac{d\phi_s}{dx}\right]_{x_j^L}^{x_j^R} H_k(s)$$

$$= \int_0^L F(x,s)\phi(x)dx - \left(\int_0^L ms^2 \, \phi(x)d + \frac{\omega_t^2 s^2}{s^2 + \omega_t^2} \sum_{j=1}^{S} m_j \, \phi_s(x_j) \right) W_b(s) \qquad (19)$$

We can substitute term m_j as $\mu m \Delta x_j$, where Δx_j is $\frac{L}{S}$. we can introduce EI term to the electromechanical term by dividing and multiplying the electromechanical term by EI. By dividing top and bottom of electromechanical term by c_p and by multiplying top and bottom by Δx_j^2, we can obtain the coupling term α. Due to the above simplifications, equation 19 can be written as shown in equation 20 and the equation of electromechanical coupling term α is given by equation 21. This term α influence the width of the bandgap formation

$$H_r(s)[s^2 + \omega_r^2] + \frac{\mu\omega_t^2 s^2}{s^2 + \omega_t^2} \sum_{k=1}^{N} \sum_{j=1}^{S} m \, \phi_k(x_j^R)\phi_s(x_j^R)\Delta x_j H_k(s)$$

$$+ \frac{\alpha}{s + \frac{Y(s)}{c_p}} \sum_{k=1}^{N} \sum_{j=1}^{S} EI \frac{\left[\frac{d\phi_k}{dx}\right]_{x_j^L}^{x_j^R}}{\Delta x_j} \frac{\left[\frac{d\phi_s}{dx}\right]_{x_j^L}^{x_j^R}}{\Delta x_j} \Delta x_j H_k(s)$$

$$= \int_0^L F(x,s)\phi(x)dx$$

$$- \left(\int_0^L ms^2 \, \phi(x)dx + \frac{\mu\omega_t^2 s^2}{s^2 + \omega_t^2} w_b(s) \sum_{j=1}^{S} m \, \phi_s(x_j)\Delta x_j \right) W_b(s) \qquad (20)$$

$$\alpha = \frac{\theta \Delta x_j}{EI c_p} = \frac{2\theta^2 h_p}{EI \varepsilon_{33}^S b} \qquad (21)$$

4. Data

In implementing numerical solution following set of data was used. PMN-PT (33% PT) piezoelectric material was used. These values were extracted from the literature [2]. Due to following data, $\alpha = 0.4580$ was obtain which is the electromechanical coupling. Data used in the numerical implementation is given in the table 1.

Term	Value	Unit
b	100	mm
L	1000	mm
h_p	0.3	mm
h_s	0.1	mm
ρ_S	2700	kgm^{-3}
ρ_p	8060	kgm^{-3}
c_S	69	GPa
$\bar{c}_{11}^E$	14.5	GPa
$\bar{e}_{31}$	-19.3	Cm^{-2}
$\bar{\varepsilon}_{33}^S$	47	nFm^{-1}
μ	1	
S	8	

In implementing the summation of modes, $N = 200$ was used. This value highly influences the accuracy of the results as discussed in the following chapters.

5. Infinite number of resonators

a. Frequency response function of the beam

When S tend to ∞, the summation due to mechanical and electromechanical resonators in the equation 20 can be approximated with Riemann sum approximation of the orthogonality condition which is given by equations 22 and 23. For a circuit with inductance, $Y(s)$ is given by $\frac{1}{Ls}$ [2]. The resonance frequency of the electromechanical resonator is given as $\omega_e^2 = \frac{1}{Lc_p}$ [2]. ω_e is the electromechanical resonance frequency. Therefore, when S goes to ∞ equation 20 can be modified as shown in the equation 24 where $H_r(s)$ can be calculated explicitly as a result of decoupling of equation 20. For the simplicity right hand side of the equation 20 will be called Q_r given by equation 25. In equation 25, the summation is replaced with an integral when S tend to ∞.

$$S \to \infty \sum_{k=1}^{N} \sum_{j=1}^{S} m\,\phi_k\left(x_j^R\right)\phi_s\left(x_j^R\right)\Delta x_j H_k(s) = H_r(s) \tag{22}$$

$$S \to \infty \sum_{k=1}^{N} \sum_{j=1}^{S} EI\, \frac{\left[\frac{d\phi_k}{dx}\right]_{x_j^L}^{x_j^R} \left[\frac{d\phi_s}{dx}\right]_{x_j^L}^{x_j^R}}{\Delta x_j}\, \frac{}{\Delta x_j}\,\Delta x_j H_k(s) = \omega_r^2 H_r(s) \tag{23}$$

$$H_r(s) = \frac{Q_r}{\left(s^2 + \omega_r^2 + \frac{\mu\omega_t^2 s^2}{s^2 + \omega_t^2} + \frac{\alpha s^2}{s^2 + \omega_e^2}\omega_r^2\right)} \tag{24}$$

$$Q_r = \int_0^L F(x,s)\phi(x)dx - \left(\int_0^L ms^2\,\phi(x)dx + \frac{\omega_t^2 s^2}{s^2 + \omega_t^2}\int_0^L m\,\phi(x)dx\right)W_b(s) \tag{25}$$

Frequency response function of the structure with an infinite number of resonators was calculated. For this purpose, equation number 24 is written in frequency domain as shown in equation 26.

$$H_r(\omega) = \frac{Q_r}{\left(-\omega^2\left(1 + \frac{\mu\omega_t^2}{\omega_t^2 - \omega^2}\right) + \omega_r^2\left(1 - \frac{\alpha\omega^2}{\omega_e^2 - \omega^2}\right)\right)} \tag{26}$$

In solving the above equation numerically, we had found several numerical errors. These issues are deeply discussed in the section 8.a of this project report. For this case plotting FRF of relative tip displacement, the linear bending force is neglected, and only base excitation is considered. Q_r term is modified to facilitate the above argument.

We can view the term $1 + \frac{\mu \omega_t^2}{\omega_t^2 - \omega^2}$ as a dynamic mass and the term $1 - \frac{\alpha \omega^2}{\omega_e^2 - \omega^2}$ as a dynamic stiffness term. These terms are negative in the region given by inequalities shown in equation 27 and 28 respectively. This effect is able to generate a bandgap in the structure with resonators in the intervals given by equations 27 and 28.

$$\omega_t < \omega < \omega_t \sqrt{1 + \mu} \tag{27}$$

$$\frac{\omega_e}{\sqrt{1 + \alpha}} < \omega < \omega_e \tag{28}$$

We can calculate equations 27 and 28 by solving the polynomial found on the denominator of equation 26 and looking the limit to the frequency ω tend to ∞, for the mechanical and electromechanical resonators case separately.

Transmissibility frequency response function (TFRF) is the transverse vibration of the beam tip per base motion as a function of the excitation frequency. In order to do that, calculated modal weight is multiplied by the modal shape of plain structure at the beam tip for each mode and summed up for each mode. Basically, it is equation 8 when $x = L$. Order to have better visualization of data we use the logarithmic scale to plot the. Bandgap related to the mechanical and electromechanical are highlighted.

When plotting the TFRF three different plots were plotted such that resonance frequency of the electromechanical resonators and resonance frequency of the mechanical resonators to be $(40\omega_1, 42\omega_1)$, $(40\omega_1, 40\omega_1)$ and $(42\omega_1, 40\omega_1)$ respectively as shown in the figures 2, 3 and 4. ω_1 is the first natural frequency of the plain structure.

The X axis and the Y axis of the figures correspond to base excitation frequency of the uniform bimorph cantilever beam normalized to the first mode frequency and transverse vibration at beam tip per base vibration respectively. In calculating the figures, 200 modes were used. It was observed that a higher number of modes provide better results which enable to distinguish clear bandgap since a greater number of modes contribute to a better approximation of analytical derivation according to the equation 8.
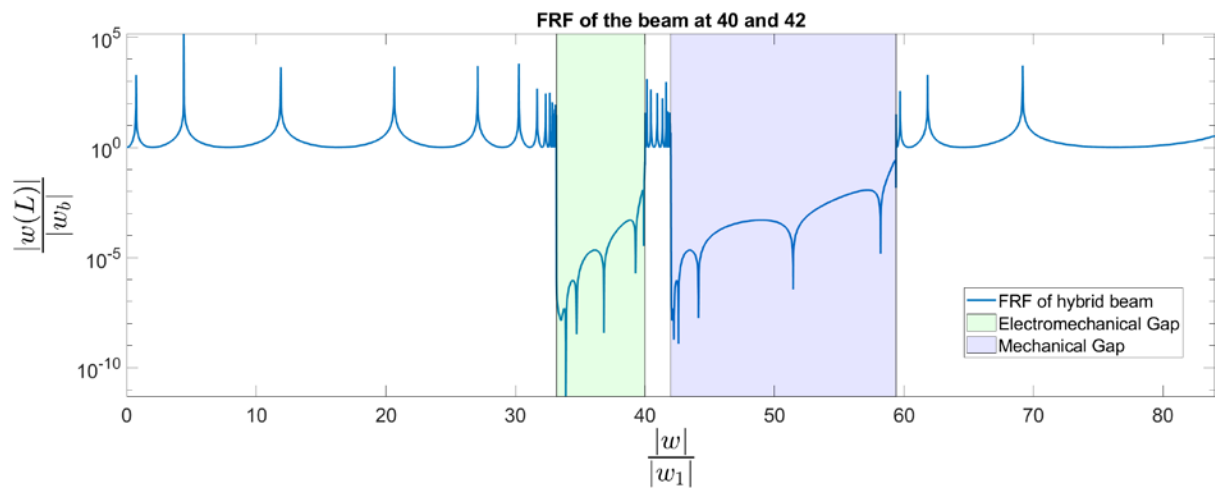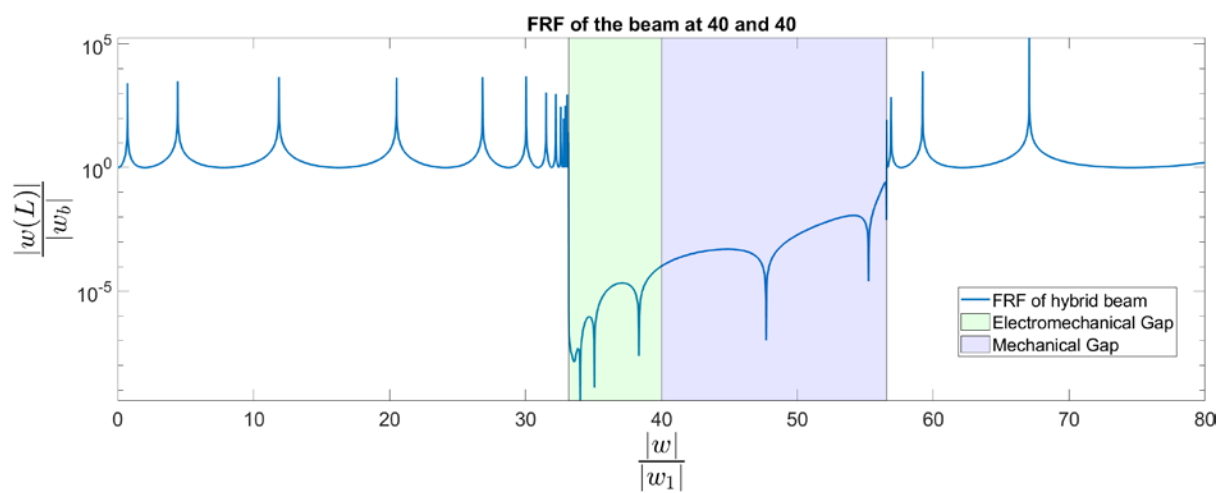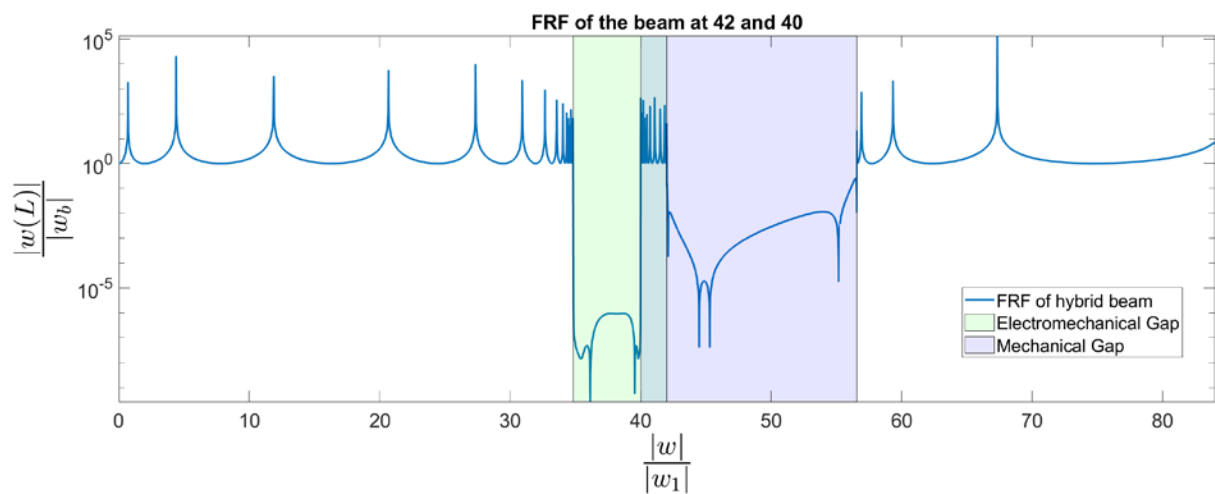
Figure 2

Figure 3

Figure 4

The bandgap in figures 2, 3 and, 4 obeys the theoretical limits of the bandgaps. These respective bandgaps are highlighted in green and purple colours for electromechanical and mechanical resonators respectively. Having the resonance frequency of both mechanical and electromechanical resonators equal, we can merge the bandgap seamlessly as shown in figure 3. The limit of the new bandgap is $\frac{\omega_e}{\sqrt{1+\alpha}} < \omega < \omega_t \sqrt{1+\mu}$, a merge of equation 27 and 28. ω_t and ω_e are the resonance frequencies of mechanical and electromechanical resonators respectively. When the resonance frequencies overlap, in the overlapped area no bandgap was observed and neither when the frequencies are distinct and not overlapping. The width of the bandgaps can be controlled by controlling α and μ values which are electromechanical coupling term and ratio of total mass added to the beam mass. Higher α and μ provide a wider bandgap. It also observed that resonance frequencies out of bandgap are changed with respect to the resonance frequencies of plain structure.

b. Transmissibility of the beam

In plotting the transmissibility of the beam, the base excitation is neglected, and linear bending force was considered. The force considered was given by equation 29 and its Laplace version is given by equation 30. F_0 is the amplitude of the force. The Q_r can presented for the above argument as shown in the equation 31.

$$
\left[
\begin{array}{ll}
f(x,t) = 0 & x \neq x_i \\[2mm]
F_0 & x = x_i
\end{array}
\right.
\tag{29}
$$

$$
\left[
\begin{array}{ll}
F(x,s) = F_0 & x = x_i \\[2mm]
F(x,s) = 0 & x \neq x_i
\end{array}
\right.
\tag{30}
$$

$$
Q_r = F_0 \phi(x_j)
\tag{31}
$$

Substituting equation 31 in equation 26 we can obtain modal weighting in frequency domain as shown in equation 32. The transmissibility can be found by using equation 33.

$$
H_r(\omega) = \frac{F_0 \phi(x_j)}{\left(-\omega^2 \left(1 + \frac{\mu \omega_t^2}{\omega_t^2 - \omega^2} \right) + \omega_r^2 \left(1 - \frac{\alpha \omega^2}{\omega_e^2 - \omega^2} \right) \right)}
\tag{32}
$$

$$
TR(\omega) = \left| \frac{W(x_{out}, \omega)}{W(x_{in}, \omega)} \right|
\tag{33}
$$

In equation 33, W is the transverse vibration. Transmissibility is simply the ratio between the transverse displacement of beam tip and the point of excitation as given by equation 33. In figure 5, Y axis shows the transmissibility of the beam when the point of the excitation moves along the beam and X axis is the normalized excitation frequency with respect to the first mode frequency. In figure 5, Y axis was normalized with the length of the beam.

In plotting figure 5, 200 modes were considered, and the number of the modes heavily influence figure 5. Figure 6 was plotted with 20 modes, and we can see the difference with respect to the figure 5. Generally higher the number of modes, better the results since equation 8 become more precise.
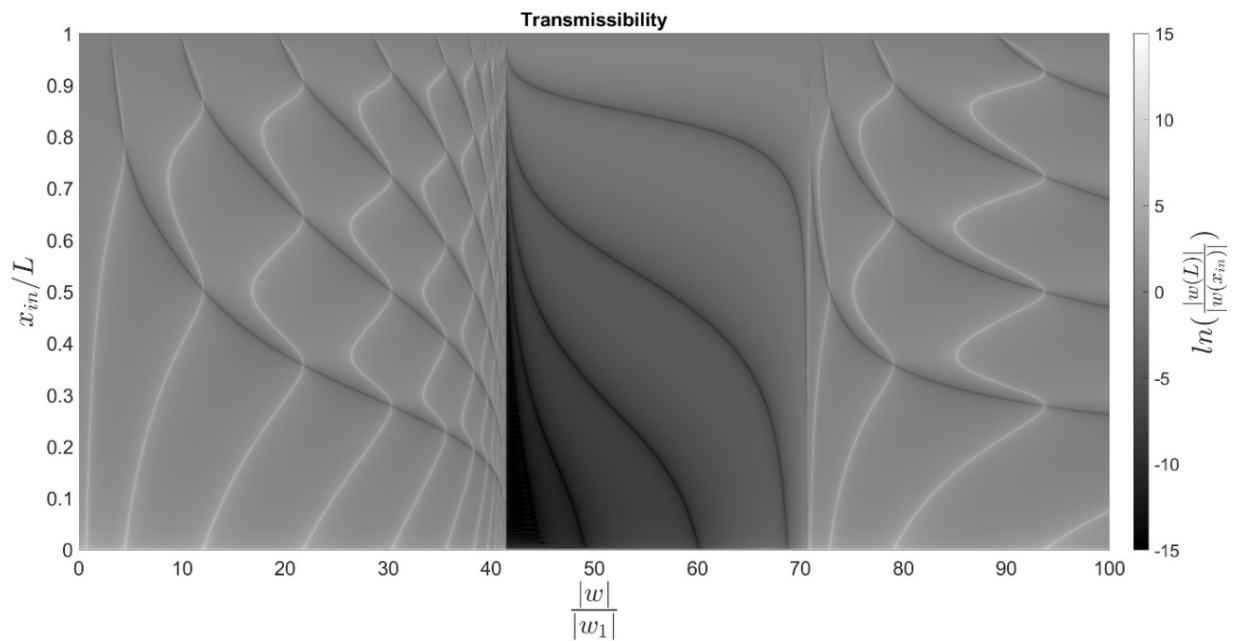
Figure 5

In figure 5, the resonance frequencies of the resonators are equal, and they were set to be $50\omega_1$, where ω_1 is the first natural frequency of the plain structure. Therefore, the bandgap is merged seamlessly. The range of frequencies where the bandgap appears are given by the inequality $\frac{\omega_e}{\sqrt{1+\alpha}} < \omega < \omega_t \sqrt{1+\mu}$. It is observed that when the excitation frequency is far away from the tip of the beam, a better bandgap is observed and the attenuation of larger. It is observed that the attenuation within the total bandgap is not equal, and the highest attenuation is observed above the frequency $\frac{\omega_e}{\sqrt{1+\alpha}}$ which is the lower bound of the bandgap due to the electromechanical resonators.
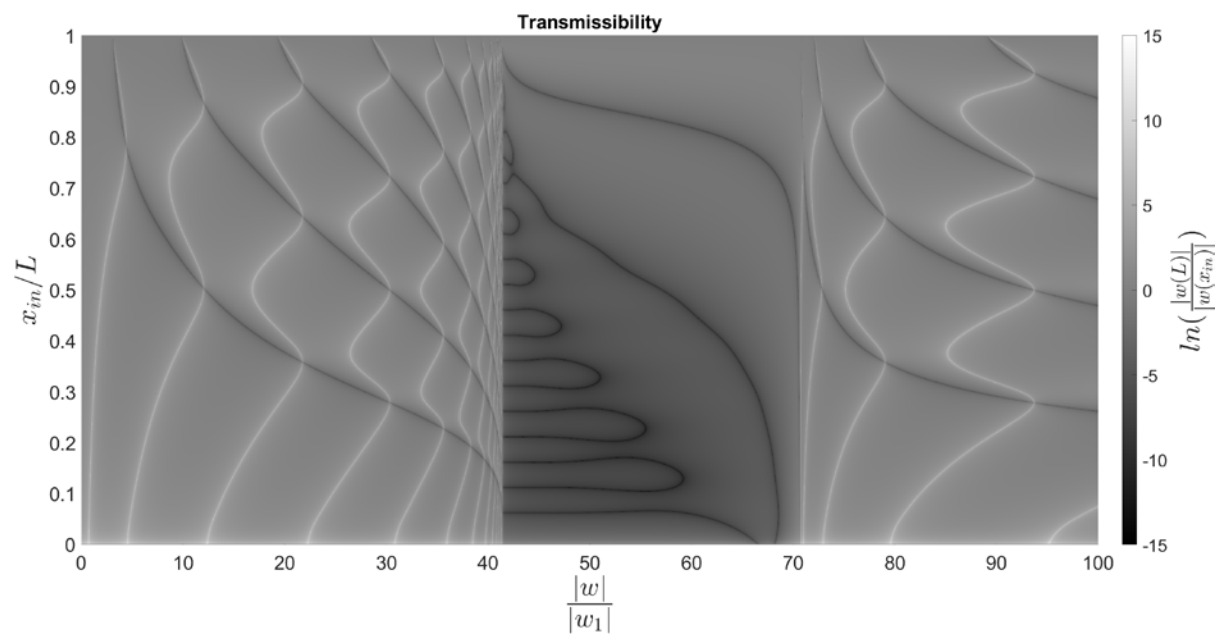
Figure 6

6. Finite number of resonators

a. Frequency response function of the beam

For the finite number of resonators, we can no longer do the sum approximation. Therefore, through the numerical procedure, we must perform the summation. The equation 20 is converted into the frequency domain as given by equation 34. Here we neglect the linear bending force, and we assume that the structure is excited only by the base excitation. The Q_r term is modified accordingly and brought to the frequency domain as shown in equation 35.

$$H_r(w) = \frac{Q_r}{-\omega^2 \left[1 + \frac{\mu\omega_t^2}{\omega_t^2 - \omega^2} M_{res} \right] + \omega_r^2 - \frac{\alpha\omega^2}{\omega_e^2 - \omega^2} K_{res}} \tag{34}$$

Where,

$$M_{res} = \sum_{r=1}^{N} \sum_{j=1}^{S} m\, \phi_s(x_j)\phi_r(x_j)\Delta x_j \quad and \quad K_{res} = \sum_{r=1}^{N} \sum_{j=1}^{S} EI \frac{\left[\frac{d\phi_r}{dx} \right]_{x_j^L}^{x_j^R} \left[\frac{d\phi_s}{dx} \right]_{x_j^L}^{x_j^R}}{\Delta x_j \; \Delta x_j} \Delta x_j$$

$$Q_r = \omega^2 \left[\int_0^L m\, \phi_r(x)dx + \frac{\mu\omega_t^2}{\omega_t^2 - \omega^2} \sum_{j=1}^{S} m\, \phi_s(x_j)\Delta x_j \right] \omega_b \tag{35}$$

By using the equation 34 and 35 $\frac{H_r}{\omega_b}$ was calculated and the obtained solution is transverse vibration of the beam tip per base motion as a function of exciting frequency as we had done before. These calculations were done for three different target frequencies and for structures having from 0 resonators to 20 resonators obtaining the figures 7, 8, and 9. The three different control frequencies were used for both mechanical and electromechanical resonators which are $20\omega_1$, $50\omega_1$, $100\omega_1$. ω_1 is the first mode frequency of the plain structure.

In figures 7, 8, and 9, X axis corresponds to number of resonators. Y axis corresponds to the excitation frequency with respect to ω_1. Colour bar represents the amplitude. Lower control frequency (resonance frequencies of the resonators) has bandgap initiated at a lower number of resonators, but its attenuation is lower than that of higher control frequency. It is observed that increasing the control frequency we need a higher number of resonators to obtain the bandgap. Bandgap due to mechanical resonators appears always with a low number of resonators compared to the electromechanical resonators. When the number of the resonators increases it tends to obey the inequalities given by the equation 27 and 28. In the hybrid structure bandgap due to the mechanical resonators have higher attenuation than the electromechanical bandgap at higher bandgap control frequency.
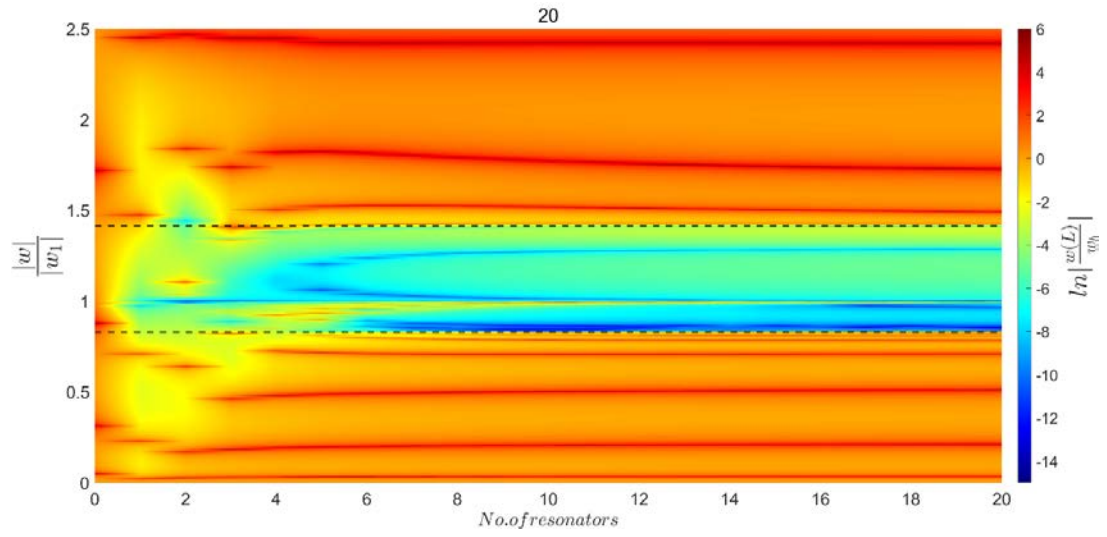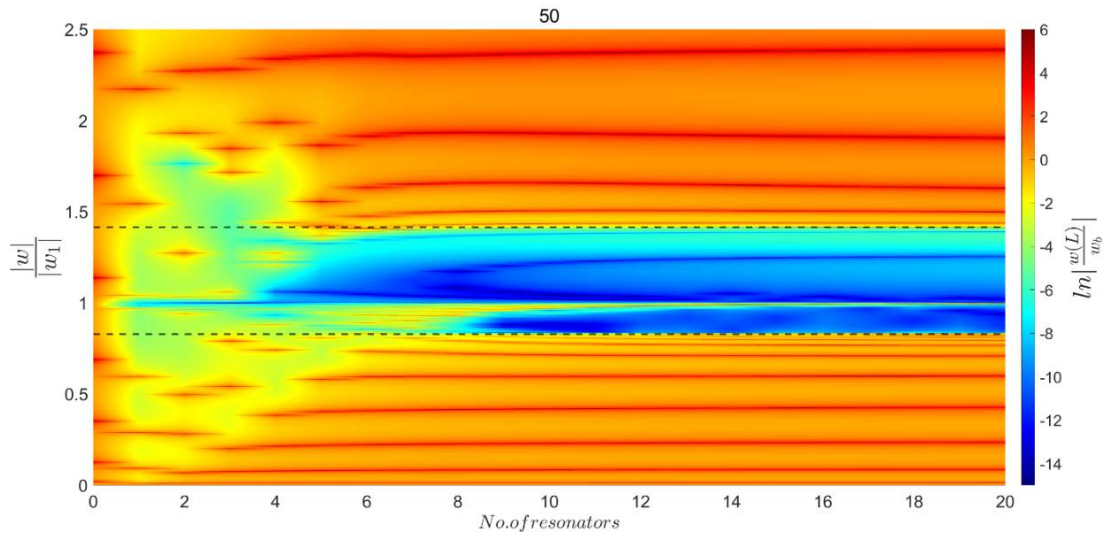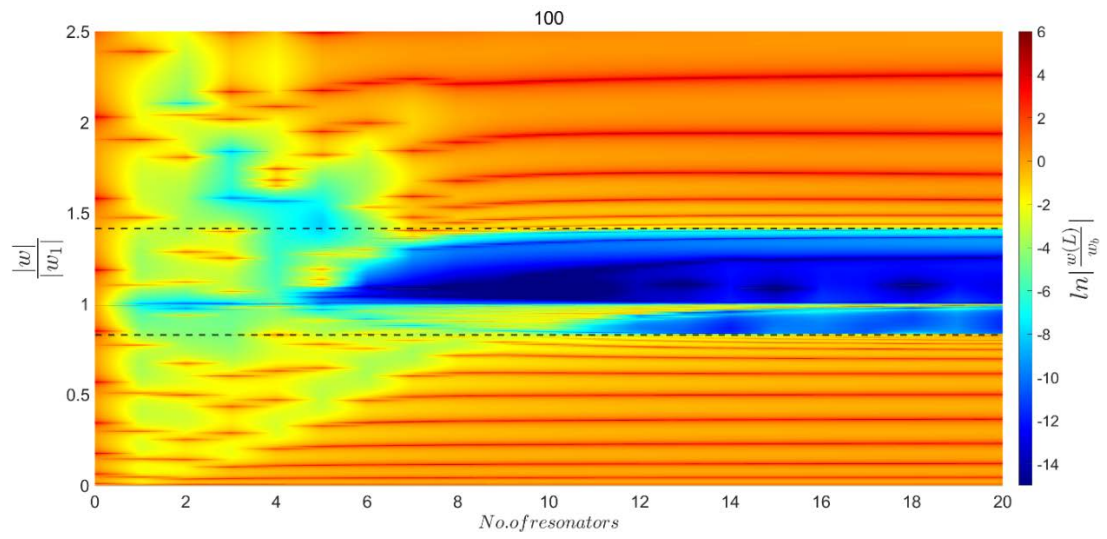
Figure 7

Figure 8

Figure 9

18

b. Damping on mechanical resonator

The frequency response of the hybrid structure with damping on the mechanical resonators is calculated. In order to consider the damping in equation 34, modify term must be introduced by the mechanical resonator. The modifying term can be identify solving the general theory for the hybrid structure with the new equation of motion for the mechanical resonator given by equation 36. The modified modal weight function is given by equation 37. In these calculations, only the base excitation is considered hence Q_r is equal to equation 35. ζ is the damping ratio and i signify imaginary.

$$m_j \ddot{u}_j + k_j u_j(t) + r_j \dot{u}_j(t) + m_j \ddot{\omega}(x_j, t) = -m_j \ddot{\omega}_b \tag{36}$$

$$H_r(w) = \frac{Q_r}{-\omega^2 \left[1 + \frac{\mu(\omega_t^2 + 2i\zeta\omega_t\omega)}{\omega_t^2 - \omega^2} M_{res} \right] + \omega_r^2 - \frac{\alpha\omega^2}{\omega_e^2 - \omega^2} K_{res}} \tag{37}$$

Where,

$$M_{res} = \sum_{r=1}^{N} \sum_{j=1}^{S} m\, \phi_s(x_j) \phi_r(x_j) \Delta x_j \quad and \quad K_{res} = \sum_{r=1}^{N} \sum_{j=1}^{S} EI \frac{\left[\frac{d\phi_r}{dx} \right]_{x_j^L}^{x_j^R} \left[\frac{d\phi_s}{dx} \right]_{x_j^L}^{x_j^R}}{\Delta x_j} \Delta x_j \tag{38}$$

By using equation 37 same as before we can calculate the transverse beam vibration at the tip of the beam per base vibration as a function of the normalized frequency and plot it.

In the case with finite number of resonators, it is observed that even having the same control frequency (resonance frequencies of the mechanical and electromechanical resonators) it is difficult to merge the bandgap seamlessly. It is evident in figure 10 there are some resonances appear at the boundaries of mechanical and electromechanical bandgaps. Figure 10 was plotted by considering 8 hybrid resonators and 200 modes.

But by introducing the damping on the mechanical resonator we can reduce this effect. TFRF is calculated for 3 different damping ratios which are $\zeta = 0$, $\zeta = 0.01$, and $\zeta = 0.02$ as shown in figure 10. The X axis of figure 10 is the base excitation frequency normalized with respect to the first mode frequency of the plain structure. The Y axis is the transverse displacement of the beam tip with respect to the base motion for each case. The graph is plotted on the logarithmic scale.

We can observe that antiresonance and resonance within the bandgap are smoothed out with the introduction of damping and increasing the damping ratio increase the smoothness. Further, the amplitude at each resonance frequencies is attenuated. Damping can be seen as dissipation of energy therefore above-mentioned attenuation is reasonable. At the boundary

of the electromechanical and mechanical bandgap, the resonances can be attenuated by using damping.
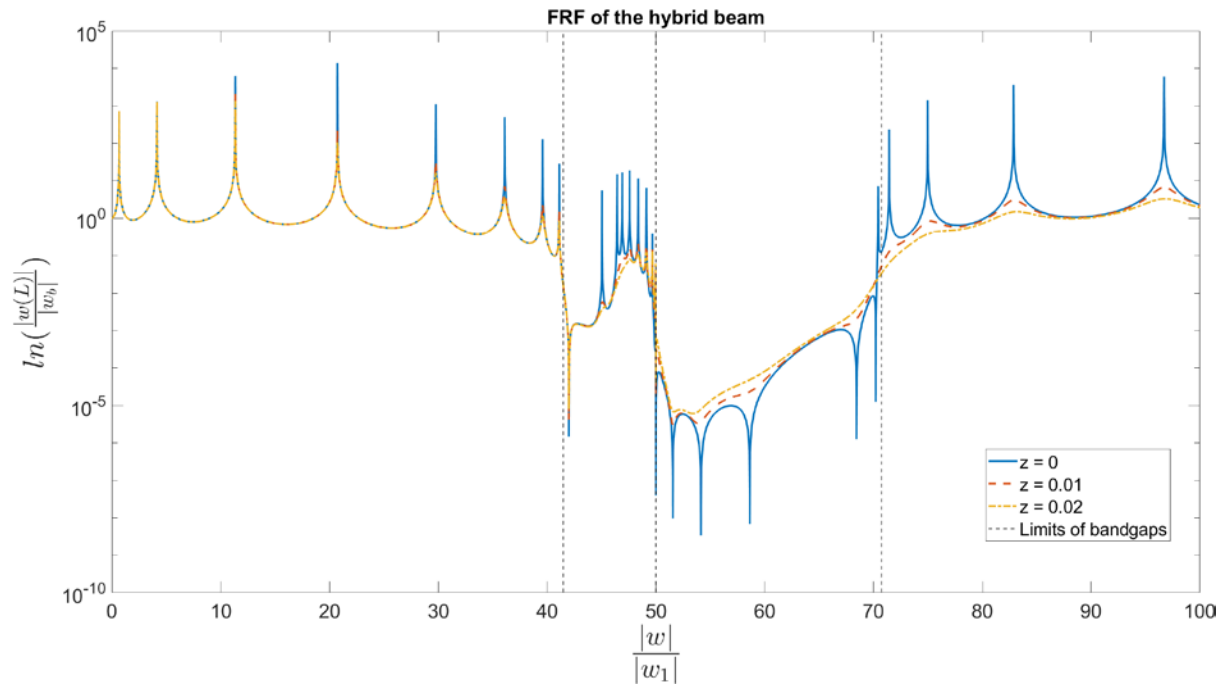

Figure 10

7. Energy Harvesting through electromechanical resonator

In order to achieve the energy harvesting through the electromechanical resonator, we connect a resistor parallel to the inductor. We assume that the resistance in all the resonators is equal. The $Y(s)$ in equation 20 for the modified system is given by equation 39 [3].

$$Y(s) = \frac{1}{sL} + \frac{1}{R} \tag{39}$$

Hence the $Y(s)$ is modified, $H_r(\omega)$ will be modified. By using equation 17 and bringing it into the frequency domain we can find the equation for the voltage in the jth resonator given by equation 40.

$$V_j(\omega) = \frac{-\theta \sum_{k=1}^{N} \left[\frac{d\phi_k}{dx}\right]_{x_j^L}^{x_j^R} sH_k(\omega)}{\left[c_{p,j} s + Y_j\right]} \tag{40}$$

For 20 resonators considering 200 modes and the resonance frequencies at $50\omega_1$, where ω_1 is the first mode frequency of the plain structure, voltage as a function of frequency calculated for the jth resonator. Figure 11 is plotted such that X axis is the normalized frequency with respect to the first natural frequency and the Y axis is the voltage per base vibration normalized with respect to the gravitational acceleration. In plotting the graph logarithmic scale was used.

Figure 11 is plotted for two different cases which are the short circuit case and the open circuit case. We can observe this phenomenon by having a small number of resistance and large resistance in the resistor respectively. When the resistance is low, the inductor becomes useless such that all the current pass-through resistor hence no global voltage increase is observed at its resonance frequency as shown in figure 11. Apart from short circuit case, we can observe in the open circuit that the voltage produce at its resonance frequency is higher as shown in figure 11.

Since we introduced the resistance into the hybrid structure, depending on the resistance the relative tip displacement is changed. Figure 12 was plotted using the same data used to plot figure 11 to observe the relative tip displacement with short circuit and open circuit. We can observe that when the resistance is low it is like only having mechanical resonators in the system. This is reasonable since having a short circuit removes the effect of the inductance. When the resistance is large the bandgap due to the electromechanical resonator appears since the current passes through the inductor. Also, we can observe the effect of the resistance throughout the mechanical band bandgap. The oscillation near the neighbourhood

of the resonance frequency of the resonator vanishes since the introduction of the resistance and this could be due to the dissipation of energy due to the resistance.
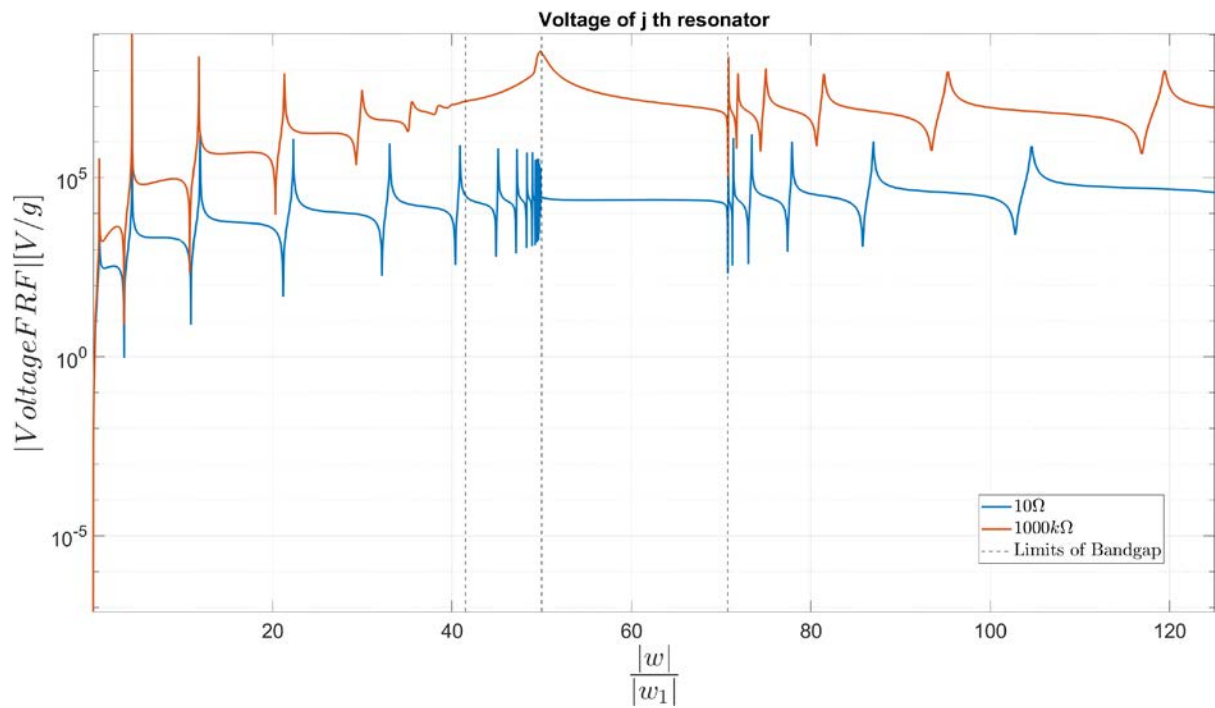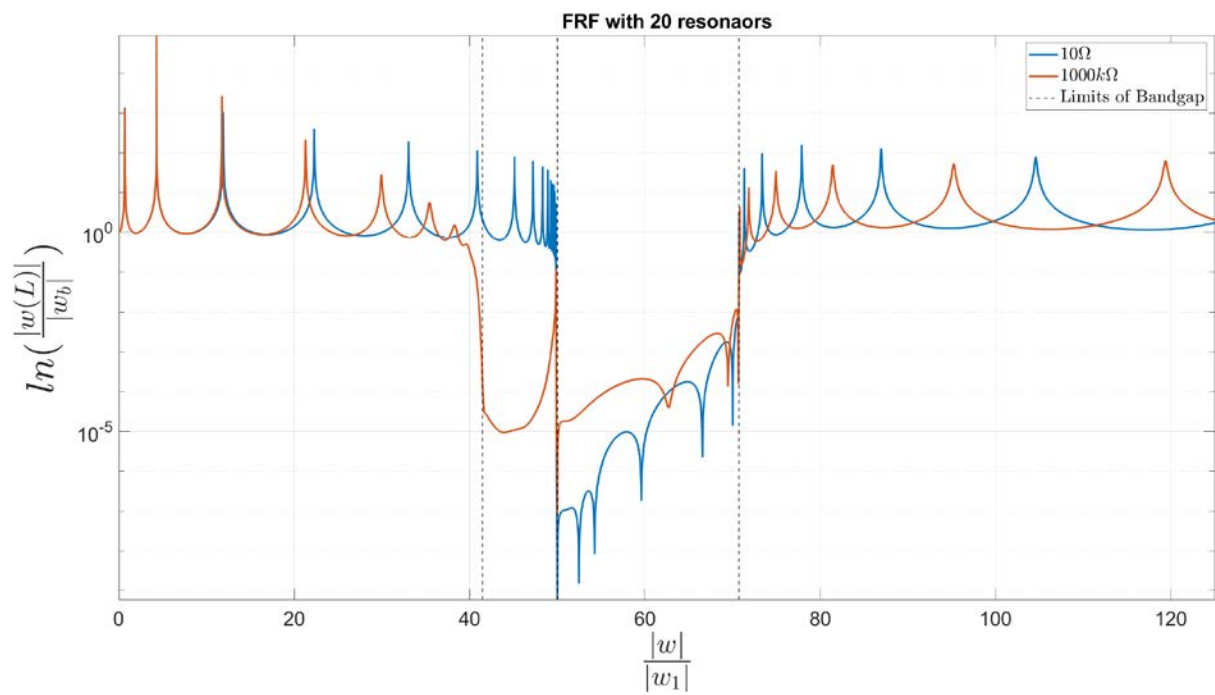

Figure 11

Figure 12

8. Numerical issues

a. Model shape approximation

In implementing numerical solutions, several numerical errors are found as a result of the numerical discretization. One of the problems was that through the numerical solution the exact shape of modal shapes of plain structure at higher modes (i.e., 20th mode) was not able to reconstruct. Equation 41 represents the mass-normalized modal shape of the plain structure which can be calculated through implementing the boundary condition for the general solution of the equation of motion of the plain structure. Figure 12 shows the mode shape of the 20th mode when it is plotted through Matlab software using equation 41. At the end of the beam, it was unable to produce a smooth curve.

$$\phi_r = \frac{1}{\sqrt{mL}}\left[\cos\left(\frac{\lambda_r x}{L}\right) - \cosh\left(\frac{\lambda_r x}{L}\right) + \left(\frac{\sin\lambda_r - \sinh\lambda_r}{\cos\lambda_r + \cosh\lambda_r}\right)\left(\sin\left(\frac{\lambda_r x}{L}\right) - \sinh\left(\frac{\lambda_r x}{L}\right)\right)\right] \quad (41)$$
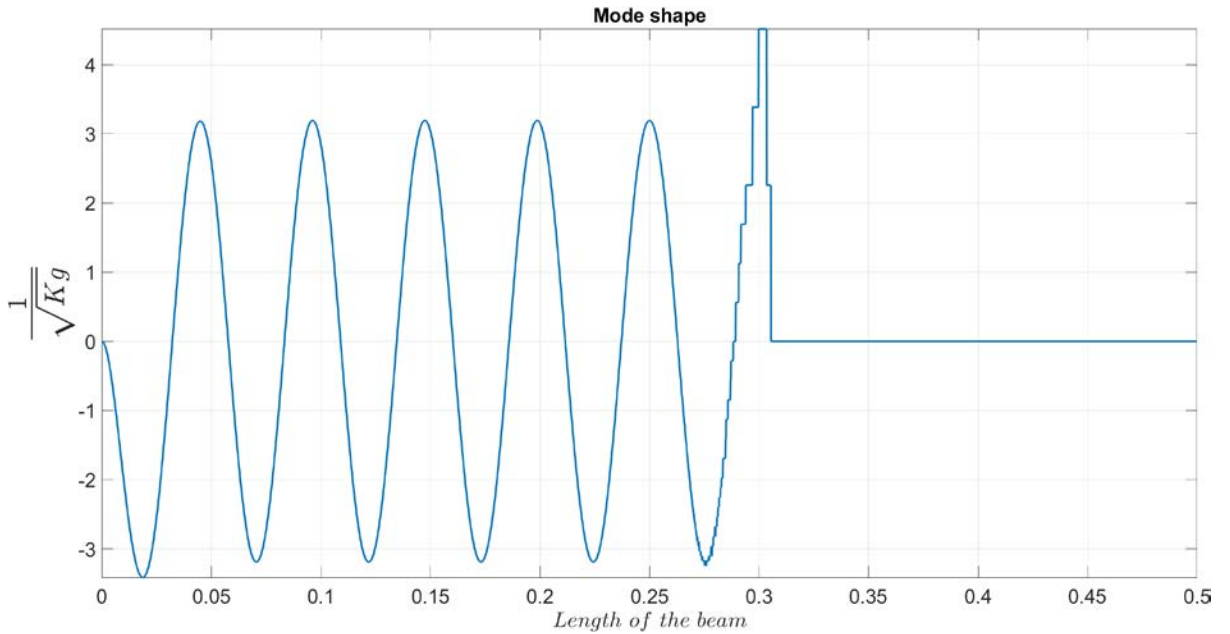

Figure 12.

In order to solve the above problem, modal shape numerical approximation was used. The approximation used in this project was obtained from the literature [4]. The modified equation of modal shape is given by equation 42. The modified modal shape can be seen in figure 13. But this approximation has an error in approximating the first few modes and this

error is about 10^{-2}. Therefore, to have better results for the first 10 modes the equation 41 was used, and for the reset of all modes equation 42 was used. This approximation is numerically valid until 200 modes.

$$\phi_r = \frac{1}{\sqrt{mL}}\left[e^{-\lambda_r x} - cos\left(\frac{\lambda_r x}{L}\right) + \left(1 + \frac{e^{-\lambda_r} - cos(\lambda_r) + sin(\lambda_r)}{sinh(\lambda_r) - sin(\lambda_r)}\right)sin\left(\frac{\lambda_r x}{L}\right)\right.$$
$$\left. -\left(\frac{e^{-\lambda_r} - cos(\lambda_r) + sin(\lambda_r)}{sinh(\lambda_r) - sin(\lambda_r)}\right)cosh\left(\frac{\lambda_r x}{L}\right)\right] \tag{42}$$
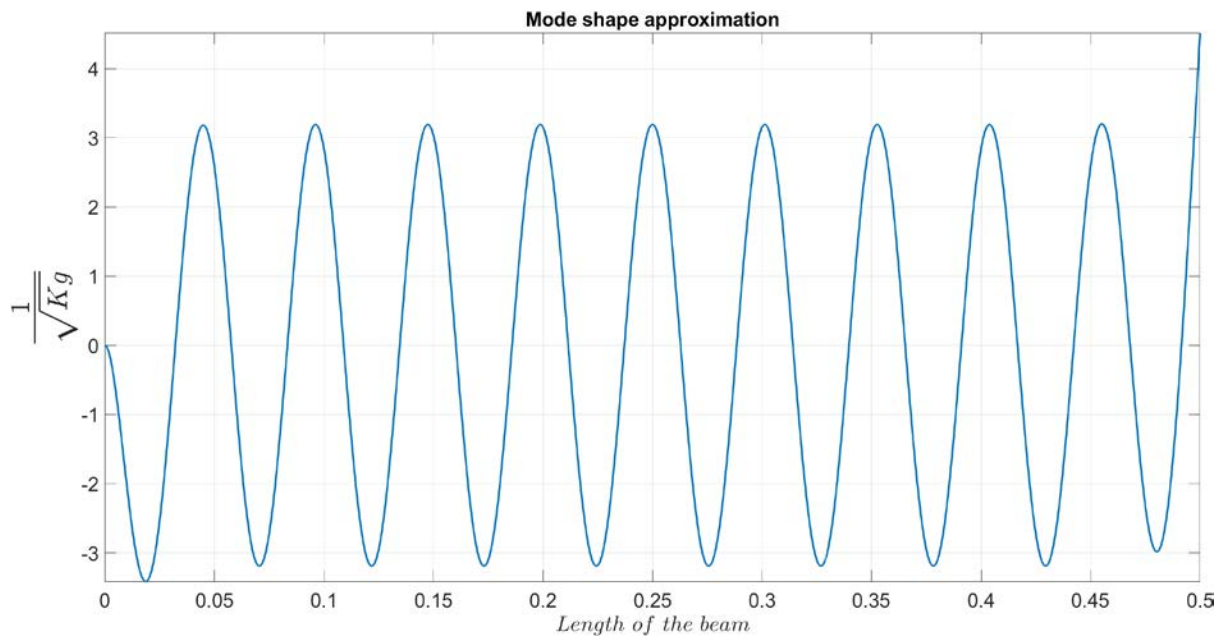

Figure 13.

b. Modal frequency approximation

In calculating the mode frequencies, the lambda values corresponding to each mode of plain structure can be calculated by solving the characteristic equation given by equation 43. The mode frequencies can be calculated by equation 44. But solving equation 43 numerically, arise numerical errors. Hence order to solve the above issue an approximated equation for lambda was used given by equation 45. This equation was extracted from the literature [4]. This equation has a higher error in the lower number of modes. Therefore, for the first 7 modes, lambda value was obtained by solving the equation 43 and for the rest of the modes equation 45 was used.

$$cos\lambda cosh\lambda + 1 = 0 \tag{43}$$

$$\omega_r = \lambda_r \sqrt{\frac{EI}{mL^4}} \tag{44}$$

$$\lambda_r \approx \frac{(2r-1)\pi}{2} \tag{45}$$

9. Reference

[1]   C. Sugino, M. Ruzzene, A. Erturk, Merging mechanical and electromechanical bandgaps in locally resonant metamaterials and metastructures, Journal of the Mechanics and Physics of Solids, Volume 116, 2018, Pages 323-333, ISSN 0022-5096.

[2]   C Sugino, S Leadenham, M Ruzzene, and A Erturk, An investigation of electroelastic bandgap formation in locally resonant piezoelectric metastructures, Smart Materials and Structures 26 (2017), no. 5, 055029.

[3]   M Alshaqaq, & A Erturk (2020). Graded multifunctional piezoelectric metastructures for wideband vibration attenuation and energy harvesting. *Smart Materials and Structures, 30(1), 015029.*

[4]   P.J.P. Gonçalves, M.J. Brennan, S.J. Elliott, Numerical evaluation of high-order modes of vibration in uniform Euler–Bernoulli beams, Journal of Sound and Vibration, Volume 301, Issues 3–5,2007, Pages 1035-1039, ISSN 0022-460X.